



HAL
open science

Towards synthetic fuels production from biomass gasification: Tar content at low temperatures

Rita Harb, Rodrigo Rivera-Tinoco, Maroun Nemer, Barbar Zeghondy, Chakib
Bouallou

► To cite this version:

Rita Harb, Rodrigo Rivera-Tinoco, Maroun Nemer, Barbar Zeghondy, Chakib Bouallou. Towards synthetic fuels production from biomass gasification: Tar content at low temperatures. *Biomass and Bioenergy*, 2020, 137, pp.105540. 10.1016/j.biombioe.2020.105540 . hal-03038821

HAL Id: hal-03038821

<https://hal.science/hal-03038821>

Submitted on 20 May 2022

HAL is a multi-disciplinary open access archive for the deposit and dissemination of scientific research documents, whether they are published or not. The documents may come from teaching and research institutions in France or abroad, or from public or private research centers.

L'archive ouverte pluridisciplinaire **HAL**, est destinée au dépôt et à la diffusion de documents scientifiques de niveau recherche, publiés ou non, émanant des établissements d'enseignement et de recherche français ou étrangers, des laboratoires publics ou privés.



Distributed under a Creative Commons Attribution - NonCommercial 4.0 International License

1 **Towards synthetic fuels production from biomass gasification: tar content at** 2 **low temperatures**

3 *Rita Harb^{a,b}, Rodrigo Rivera-Tinoco^{a,*}, Maroun Nemer^a, Barbar Zeghondy^b, Chakib Bouallou^a*

4 ^a MINES ParisTech, PSL Research University, Centre for energy efficiency of systems (CES),
5 60 Bd St Michel, F-75006 Paris, France. rita.harb@mines-paristech.fr
6 rodrigo.rivera_tinoco@mines-paristech.fr maroun.nemer@mines-paristech.fr
7 chakib.bouallou@mines-paristech.fr

8 ^b School of Engineering, Holy Spirit University of Kaslik (USEK), Jounieh, Lebanon.
9 barbarzeghondy@usek.edu.lb

10 * Corresponding author: rodrigo.rivera_tinoco@mines-paristech.fr, Centre Efficacité
11 Energétique des Systèmes (CES), 5, rue Léon Blum, 91120 Palaiseau, France.

12 **Abstract**

13 Biomass conversion into biofuels and biogas is a promising way for power and heat generation.
14 Lately, research has focused on the production of biomethane based on biomass gasification
15 followed by methanation as an alternative to fossil natural gas. The challenge of this process
16 remains in the intensive gas cleaning and required tar removal. In order to study tar removal
17 from the producer gas downstream biomass gasification, solid–vapor and liquid–vapor
18 equilibrium must be known for different tar concentrations, ranging between 0.001 and 100
19 g.Nm⁻³. To assess tar removal by condensation at low temperatures, psychrometric charts are
20 developed. Since the composition of tar is complex, toluene, phenol, indene, naphthalene and
21 fluoranthene are selected as tar representatives. Each component is studied separately in four
22 different producer gas compositions formed mainly of hydrogen, carbon monoxide, carbon
23 dioxide and methane in addition to water and nitrogen. Methods for calculating saturation,
24 isenthalpic and constant relative concentration lines are presented. Psychrometric charts of the
25 different tar components are finally plotted at atmospheric pressure. Results show that
26 temperature of 196.15 K is required to reduce the tar content to 0.001 g.Nm⁻³.

27 Keywords: tar removal, biomass gasification, thermodynamic properties, psychrometric chart.
28

29 **1. Introduction**

30 With the growing interest in fighting against global warming and carbon dioxide emissions,
31 researchers are looking to replace fossil fuels by renewable energy sources. Biomass is one of
32 these energy sources that can serve as a fossil fuel alternative. Converting biomass into
33 bioenergy can be done through biomass gasification. Gasification process converts organic
34 matter into a mixture of gas, tar and char using steam, oxygen, or air as a gasifying agent. The
35 gas is a mixture of carbon monoxide (CO), carbon dioxide (CO₂), hydrogen (H₂), steam (H₂O),
36 nitrogen (N₂) and methane (CH₄) in addition to tar vapors and some other impurities [1]. This
37 gas mixture is known as producer gas and its composition depends on the used gasifying agent as
38 well as on the gasifier type. The end use of the producer gas is limited due to the formation of
39 multiple by-products, such as NO_x, SO_x, fly ashes and tars within the gasification process [2].

40 Among the pollutants, tar removal remains the hardest one to deal with, forming the main
41 drawback of biomass gasification [3]. Tar removal can be carried out inside the gasifier (primary
42 method) or downstream the gasifier (secondary method). As the temperature decreases in the
43 downstream equipment, tars in the gas phase will condense forming a sticky deposit that foul,
44 plug and block heat exchangers, engines and filters. Moreover, tar is one of the main precursors
45 for carbon formation causing catalytic deactivation due to coke deposition [4,5].

46 The allowable tar content remaining in the producer gas after its treatment is defined by the
47 desired application [2,6]. Lower restrictions on tar concentration are set for combined heat and
48 power generation (CHP), while much stricter limitations are defined for chemical synthesis
49 processes involving a catalyst, such as Fischer-Tropsch, methanation and methanol synthesis. As
50 for CHP, it is enough to reduce the dew point of the tar to a temperature below the lowest one in
51 the process to avoid its deposition. While for chemical synthesis, the catalyst is easily
52 deactivated due to the presence of tar even at low concentrations. At temperatures lower than
53 1373 K, tar and light hydrocarbons are decomposed into coke that deactivates catalysts [4].

54 Recently, production of methane based on biomass gasification is gaining attention as a possible
55 route for replacing fossil natural gas. Combining a methanation step with biomass gasification
56 requires intensive gas cleaning and compression. To ensure a proper operation, the tar content
57 remaining in the producer gas prior to the methanation step should be less than 1 mg.Nm⁻³ [7].

58 Tar is defined, according to the tar measurement protocol [8], as hydrocarbons with molecular
59 weight higher than benzene. It is hard to predict the composition of the tar produced during
60 gasification since it depends on many factors such as the type of biomass, gasifying agent,
61 reactor type, operating temperature and pressure. Thus, to facilitate the comprehension of tar
62 composition, tar can be classified according to different characteristics. The most adapted
63 classification is presented in Table 1 where tar compounds are divided into 5 classes according to
64 their condensability and solubility.

65 After biomass gasification, the tar content in the producer gas varies between 1 g.Nm⁻³ and
66 100 g.Nm⁻³ according to the adapted process [10] even if primary methods for tar removal were
67 integrated within the gasifier. Thus, in all cases, secondary methods are required to reduce the tar
68 content to 1 mg.Nm⁻³. Up to now, very few researchers were able to reduce the tar content to this
69 level. The elimination of tar by a single step via a physical/mechanical method is not efficient
70 [3,11] and results in a tar content between 5 g.Nm⁻³ and 30 g.Nm⁻³. Combining two physical
71 methods for tar treatment increases its removal efficiency and yields a producer gas with a tar
72 content around 250 mg.Nm⁻³, noting that benzene and toluene were not taken into account [12].
73 Tar reduction via thermal cracking reduces the tar content to a value between 5 and 7 g.Nm⁻³ at
74 high temperatures (1523 K) leading to a high operating cost [13]. Catalytic cracking seems to be
75 a promising method for tar reduction. This method eliminates around 99% of tars, yielding a tar
76 content of 0.16 g.Nm⁻³. However, the high tar removal rate is limited in time due to the rapid
77 deactivation of the catalyst within few hours of operation as a result of coke deposition [14,15].
78 The highest tar removal efficiencies were achieved by combining at least two operational units.
79 The first unit is assimilated to a pre-treatment step. It increases the lifetime of the second step
80 and reduces its cost by removing the heavy fraction of tar, while lighter tar compounds are being

81 removed in the second step. Some examples of these two-step techniques are OLGA, which
 82 combines a collector followed by an absorber [16], oil or water scrubber followed by activated
 83 carbon bed [17], thermal cracking followed by an adsorption bed [18] and absorption followed
 84 by catalytic cracking [19]. It was also seen that the reduction of tar content in most of the cases
 85 was insufficient for combining gasification and methanation.

86 **Table 1**
 87 Tar classification with respect to their molecular weight [3,6,9].

Tar Class	Class Name	Property	Compounds
1	GC ^a -undetectable tar	Very heavy tars compounds that cannot be detected by GC	Determined by subtracting the GC-detectable tar fraction from the total gravimetric tar
2	Heterocyclic	Tar containing hetero atoms; very soluble in water	Pyridine, phenol, cresols, quinoline, isoquinoline, dibenzophenol
3	Light aromatic (1 ring)	Light hydrocarbons with single ring, do not pose a problem regarding condensability and solubility	Toluene, ethylbenzene, xylenes, styrene
4	Light PAHs ^b compounds (2–3 rings)	2 and 3 rings, condense at low temperature at very low concentrations	Indene, naphthalene, methylnaphthalene, biphenyl, acenaphthalene, fluorene, phenanthrene, anthracene
5	Heavy PAHs compounds (4–7 rings)	3 rings and more, condense at high temperatures even at low concentrations	Fluoranthene, pyrene, chrysene, perylene, coronene

88 ^aGas Chromatography

89 ^bPolyaromatic Hydrocarbons

90 The potential use and temperature ranges of the two steps low temperature removal process, for
 91 reducing the tar content down to 1 mg.Nm⁻³, is assessed based on the condensing temperatures of
 92 tars. The first step operates at room temperature, while the second one operates at lower
 93 temperatures. Adapting low temperature ensures the condensation of tars by cooling the producer
 94 gas to a temperature below tar dew point for a concentration of 1 mg.Nm⁻³. Different ways could
 95 be adapted in order to cool the producer gas. Suggesting the use of low temperature tar removal
 96 offers the possibility to reduce dramatically the content of light tars in the producer gas, while
 97 generating condensate fractions of potential market value. Handling condensates, however,
 98 remains the main drawback of low temperature tar removal. Formation of solid phase layers
 99 could lead to clogging of heat exchangers, as well as a dramatic reduction on heat transfer. For
 100 this last, the energy efficiency of the process would decline rapidly and render the process
 101 economically unviable. Managing the solid phase formation in heat exchangers is a topic for
 102 which technological solutions may be available, for example, de-waxing pig systems (pipe
 103 cleaning). Another option is to cycle the temperature of heat exchangers. However, the analysis
 104 of such solutions are beyond the scope of this paper.

105

106 In order to analyze the condensation behavior of tar components at low temperature and assess
107 the energy required to condense tar compounds, psychrometric charts for tar components in
108 producer gas are plotted. Aspen Properties V10 was used to find the phase equilibrium
109 composition at saturation, as well as assessing the impact of gas mixtures compositions at
110 different temperatures. Equations were developed for calculating the enthalpy of mixtures and
111 the constant relative concentration lines. As mentioned earlier, the producer gas is a multi-
112 component mixture of CO, CO₂, H₂, N₂, CH₄, H₂O and some impurities. This composition is
113 affected by the gasification process and its parameters. The psychrometric charts are used to
114 illustrate the tar content in the producer gas at different temperatures and the energy required for
115 condensing tars at different concentrations.

116 As a part of the state of the art, an open source tool developed by the Energy research Center of
117 the Netherlands (ECN) is available online [20]. This tool enables the calculations of the dew
118 point for a single tar component or a mixture of tar components. It was developed to calculate the
119 temperature at which tar condensation starts for a given tar content expressed in g.Nm⁻³ on wet
120 basis [21]. Tar vapors are assumed as ideal gas and have an ideal mixing behavior. The main
121 disadvantage of this tool is that the composition of the producer gas is not well defined and
122 cannot be modified; hence, dew point calculations are limited.

123 In order to study the impact of the producer gas composition on the condensation behavior of tar
124 components, the dew point of tar components is studied for four different producer gas
125 compositions. Those compositions are selected in a way to cover producer gas compositions
126 obtained from several types of gasifiers and gasifying agents. This enables the comparison of the
127 simulated results with those obtained from the ECN tool. Then, a special attention will be given
128 to the energy required for the condensation of tar by finding the enthalpy of mixtures at several
129 points. The selected physical property method to be used in Aspen simulations and calculations
130 is Non-Random Two-Liquid model (NRTL) since it can handle any mixture of polar and non-
131 polar components. It is widely used for phase equilibria calculations (vapor-liquid and liquid-
132 liquid equilibrium) [22].

133 This paper is organized as follows: methodology and assumptions are presented in section 2,
134 results are shown in section 3; finally, conclusions are drawn and perspectives are provided in
135 section 4.

136 2. Assumptions and methodology

137 In this paper, four producer gas compositions are considered in order to study their impact on tar
138 dew point. Single tar component will be considered at each time. The selection criteria of tar
139 components and producer gas composition are explained later on.

140 2.1. Tar representative components

141 Since tar is a complex mixture, some tar compounds are selected as representatives components
142 per class for which psychrometric charts are plotted separately. The criteria for the selection of
143 tar representative components are:

- 144 • the lightest component in each class should be selected, thus the rest of the components in
145 the same class will condense eventually at higher temperatures.
- 146 • the fraction of the component should not be negligible.

147 Table 2 summarizes some physical properties, the class and the mass percentage of the most
148 common components forming the tar. Based on the selection criteria, it can be deduced from
149 Table 2 that tar representative components are phenol for class 2, toluene for class 3, indene and
150 naphthalene for class 4 and fluoranthene for class 5. Two components from class 4 were
151 considered since indene is the lightest one, while naphthalene is present in an important amount
152 and it was considered as tar representative in other studies [11,23,24].

153 **Table 2**
154 Physical properties of common tar components.

Component	Boiling point (K)	Freezing point (K)	Molecular weight (g.mol ⁻¹)	Class	Mass percentage (%) excl. benzene ^[25-27]
Benzene	353.24	278.68	78.11		
o-cresol	464.15	304.19	108.10	2	1-10
2,6-xylene	474.22	318.76	122.10	3	0.5-2.5
Toluene	383.78	178.18	92.13	3	8-24
o-xylene	411.51	286.41	106.10	3	1-10
Indene	455.77	271.70	116.16	4	2-12
Phenol	454.99	314.06	94.11	2	6-12
Naphthalene	491.14	353.43	128.17	4	10-30
2-methyl-naphthalene	514.26	307.73	142.19	4	4
Biphenyl	528.15	362.65	154.20	4	0-2
Acenaphthalene	543.15	342.35	152.19	4	3-7
Acenaphthene	550.54	366.56	154.20	4	0.5
Fluorene	570.44	387.94	166.21	4	0-2
Phenanthrene	610.03	372.38	178.22	4	2-4
Anthracene	615.18	488.93	178.22	4	0.2-4
Fluoranthene	655.95	383.33	202.25	5	1-2.5
Pyrene	667.95	423.81	202.25	5	0-2

155

156 **2.2. Producer gas composition**

157 As previously mentioned, different producer gas compositions are studied in order to check their
158 impact on the dew point of tar components. The main variation in the composition is the mole
159 fraction of steam (H₂O) and nitrogen (N₂). Steam gasification, for direct and indirect gasifier,
160 yields a producer gas with a high moisture content (30 to 60 mol% on wet basis). While air
161 gasification yields a producer gas with a high nitrogen content (40 to 60 mol% on dry basis). The
162 molar fraction of the remaining components is also affected by the gasifying agent. However,
163 this variation is minor in comparison with the variation of the steam and nitrogen content. Table
164 3 illustrates the different producer gas compositions used in the calculations to build the
165 psychrometric charts. The first case in Table 3 corresponds to a dual fluidized bed (DFB) gasifier
166 or indirect gasifier where wood-based biomass is being gasified using steam as the gasifying
167 agent [17]. This gasifier yields a producer gas composition suitable for methanation purposes, as
168 it is inert free with high hydrogen to carbon ratios [23,28]. The second and the third cases
169 correspond to a bubbling fluidized bed gasifier operating with air as a gasifying agent. Case 2
170 [29] corresponds to the gasification of pine wood at 1073 K with an equivalence ratio (*ER*) of
171 0.25. For case 3 [30], refused-derived fuel (RDF) is gasified at 1093 K with an *ER* equal to 0.21.
172 The last case (case 4) represents a sawmill waste downdraft gasifier that uses air as a gasifying
173 agent yielding a producer gas with a low water and high inert contents [31]. The calculated dew
174 points of tar compounds are compared with those obtained from the online tool provided by ECN
175 for the same tar concentration. The composition of the producer gas used by ECN for the
176 calculations of the tar dew point based on tar concentration is not given, but the calculations
177 were based on an atmospheric bubbling fluidized bed gasifier operating at 1123 K. The
178 calculation of tar dew point, forming the saturation line, is explained in the sequel.

179 The presence of large amounts of water in the producer gas affects tar dew point as well as the
180 enthalpy, mainly for temperatures lower than the water dew point. The initial tar content was set
181 to 100 g.Nm⁻³. Note that the presence of water in the mixture imposes the use of a suitable
182 property method for polar mixtures. In this paper, NRTL is used.

183 **Table 3**
184 Different raw gas compositions in wet basis used for the calculation of tar dew point.

	Case 1 [17]	Case 2 [29]	Case 3 [30]	Case 4 [31]
H ₂ , mol%	27.8	9.6	6.0	11.0
CO, mol%	16.7	14.4	10.9	20.0
CO ₂ , mol%	13.8	11.2	12.3	10.0
CH ₄ , mol%	6.0	4.0	5.7	3.0
C ₂ H _n , mol%	1.6	2.0	4.6	-
N ₂ , mol%	3.7	38.8	48.0	50.0
H ₂ O, mol%	30.4	20.0	12.5	6

185 **2.3. Saturation and constant relative concentration lines**

186 Calculations are based on an initial concentration of 100 g of tar.Nm⁻³ of raw gas for each tar
187 component. This concentration was selected since it is equal to the highest tar level that could be

188 obtained from the gasification. In this section, “raw gas” term corresponds to the mixture of
 189 components forming the producer gas excluding tar compounds. Same calculations are repeated
 190 for each one of the previously selected tar components: phenol, toluene, indene, naphthalene and
 191 fluoranthene.

192 Points of the saturation line for each case were calculated at first. The saturation line, liquid-
 193 vapor above the triple point and solid-vapor below it, represents the limit at which tar
 194 condensation in the producer gas starts. The vapor fraction (VF) was calculated at different
 195 temperatures (T_i) in order to detect the temperature at which condensation begins ($VF \neq 1$). At
 196 this temperature, the gas phase molar fraction (y_j) was calculated to compute the amount of tar
 197 condensed using a defined property method in Aspen Properties, where j represents the different
 198 components of the producer gas. The amount of tar remaining in the gas phase is calculated
 199 according to Eq (1) and Eq (2) where w_{tar} is defined as the tar content, in $\text{kg}\cdot\text{kg}^{-1}$ raw gas, and it
 200 is equal to the ratio of tar mass (m_{tar}) to the raw gas mass ($m_{raw\ gas}$). Tar concentration (C_{tar}) is
 201 deduced from Eq (3) in mg of $\text{tar}\cdot\text{Nm}^{-3}$ of raw gas. Same calculations are repeated for different
 202 temperatures. The latter decreases with an interval of 10 K until reaching a tar concentration of 1
 203 mg of $\text{tar}\cdot\text{Nm}^{-3}$ of raw gas. The equations presented below (from Eq (1) to Eq (7)) are analogous
 204 to the equations used for the psychrometric chart of humid air, however applied for other
 205 components.

$$P_{sat}(T_i) = y_{tar}(T_i) \cdot P_{total} \quad (1)$$

$$w_{tar} = \frac{m_{tar}}{m_{raw\ gas}} = \frac{P_{sat}(T_i)}{P_{total} - P_{sat}(T_i)} \cdot \frac{M_{tar}}{M_{raw\ gas}} \quad (2)$$

$$C_{tar} = \frac{w_{tar}}{\rho_{raw\ gas}} \cdot 10^6 \quad (3)$$

206 where M_{tar} and $M_{raw\ gas}$ are respectively tar and raw gas molecular masses in $\text{g}\cdot\text{mol}^{-1}$, P_{sat} is the
 207 saturated tar partial pressure in the raw gas in Pa, P_{total} is the total mixture pressure and it is equal
 208 to the atmospheric pressure in Pa and $\rho_{raw\ gas}$ is the density of the raw gas in $\text{kg}\cdot\text{m}^{-3}$.

209 Constant tar relative concentration (ϕ) curves are then plotted. ϕ is expressed in Eq (4) and it is
 210 equal to the ratio of the tar partial pressure in the raw gas (P_{tar}) to the saturated tar partial
 211 pressure at the same temperature (T_i). To plot those curves, tar partial pressure was calculated at
 212 each T_i for a fixed value of ϕ according to Eq (5). Tar vapors are assumed to behave as ideal
 213 gases. For each value of ϕ , ranging between 10% and 90%, and for a total pressure of one
 214 atmosphere, the tar content was calculated for different temperatures according to Eq (6).
 215 Finally, tar content is plotted against the temperature for each value of ϕ .

$$\phi = \frac{P_{tar}(T_i)}{P_{sat}(T_i)} \quad (4)$$

$$P_{tar}(T_i) = \phi \cdot P_{sat}(T_i) = \phi \cdot y_{tar} \cdot P_{total} \quad (5)$$

$$w_{tar} = \frac{\phi \cdot y_{tar}(T_i)}{1 - \phi \cdot y_{tar}(T_i)} \cdot \frac{M_{tar}}{M_{raw\ gas}} \quad (6)$$

2.4. Saturation enthalpy and isenthalpic lines

Isenthalpic lines help in finding, at any condition, the enthalpy of the mixture. They join several points together having an equal enthalpy. The enthalpy of the gas mixture is calculated per kilogram of dry raw gas. Calculations begin by finding the enthalpy at saturation. Plotting enthalpies at saturation versus the temperature yields the saturation enthalpy line. In Fig. 1, points 1 and 2 of the saturation line are considered. Tar contents, dew points and the enthalpies of those points are known. Note that point 1 has the highest dew point. A constant tar content line, drawn as a horizontal line starting from point 2, intersects with the constant enthalpy line of point 1. The intersection point is denoted as point 3. Consequently, the following equations can be concluded: $h_1=h_3$, $w_{tar,2}=w_{tar,3}$ and $w_{wat,2}=w_{wat,3}$ where w_{wat} corresponds to the water content, in kg.kg^{-1} raw gas. The enthalpy of the raw gas at any point, expressed in kJ.kg^{-1} , is given in Eq (7). This equation describes the conventional enthalpy calculation at dry bulb conditions considering mainly gas and liquid phases. As operating temperatures considered for tar removal are below 273 K, the risk of ice and tar deposit formation exists. Even though preliminary calculations show limited discrepancies between calculated and existing data on psychrometric charts for water, the assessment of the impact of considering L-V or S-L-V phases on enthalpy calculations including water and tars is needed. This is beyond the scope of this work and will be dealt with in future as enthalpy miscalculations could lead to overconsumption of cooling utilities, in particular at low temperatures.

$$h = C_{p,raw\ gas} \cdot T_{DB} + w_{tar} [h_{fg,tar(273\ K)} + C_{p,tar,vap} \cdot T_{DP,tar}] + w_{wat} [h_{fg,wat(273\ K)} + C_{p,wat,vap} \cdot T_{DP,wat}] \quad (7)$$

where $C_{p,raw\ gas}$ is the heat capacity of the mixture excluding water and tar component, $C_{p,tar,vap}$ and $C_{p,wat,vap}$ are respectively the heat capacity of the tar component and water in the vapor phase expressed in $\text{kJ.kg}^{-1}.\text{K}^{-1}$, T_{DB} is the dry bulb temperature expressed in K, $h_{fg,tar}$ is the latent heat of vaporization or the latent heat of sublimation of tar component depending on its triple point expressed in kJ.kg^{-1} , $h_{fg,wat}$ is the latent heat of vaporization of water expressed in kJ.kg^{-1} and T_{DP} is the dew point temperature expressed in K.

By solving Eq (7) for points 1, 2 and 3, Eq (8) can be deduced. The latter is solved for $T_{DB,3}$, thus the coordinates of a new point on the isenthalpic line are found. To reach better accuracy, three-to-four points are considered in the plot of the constant enthalpy line.

$$h_3 - h_2 = C_{p,raw\ gas,3} \cdot T_{DB,3} - C_{p,raw\ gas,2} \cdot T_{DB,2} \quad (8)$$

244

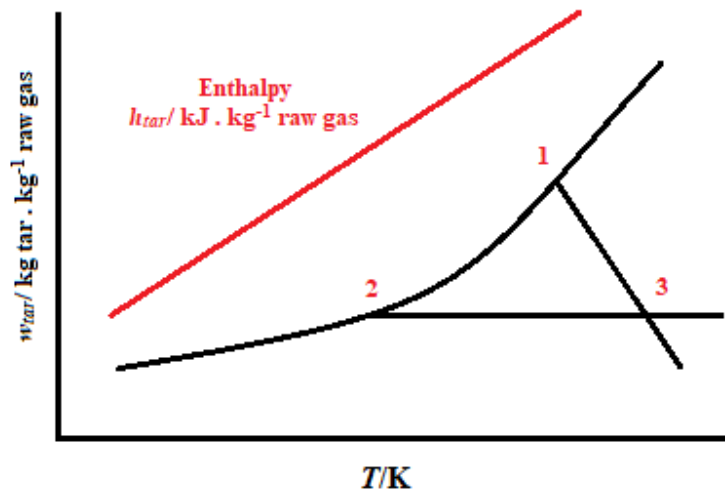


Fig. 1. Illustration of the constant enthalpy line calculations.

245 When the condensation takes place at a temperature lower than the triple point (in solid phase),
 246 the built-in correlations in Aspen Properties do not consider the solid phase condensation and
 247 may yield non-accurate results. Studying the solid condensation behavior for each tar compound
 248 separately is very time consuming since the composition of tar is complicated and encloses too
 249 many compounds. In addition, developing a solid phase characteristic curve for all the
 250 compounds is not necessary. Therefore, we investigate in a general way to develop a solid
 251 condensation characteristic curve by expanding the liquid condensation laws into the solid phase.
 252 To justify the decision of expanding the laws into the solid phase, a comparison between the
 253 vapor pressure obtained using Aspen and that found in the literature for multiple compounds is
 254 done for a defined temperature interval below the triple point. The comparison was done for
 255 fluoranthene, naphthalene and phenol. Note that a comparison with the solid vapor pressure of
 256 indene was not done since the latter was not found in the literature review. Similarly for the
 257 toluene, which triple point is too low. It is important to mention that the comparison was done
 258 based on dry basis raw gas composition. Otherwise, the curves could not be compared since the
 259 condensation of water affects the tar condensation.

260 **3. Results and discussion**

261 **3.1. Solid – gas equilibrium**

262 A comparison between experimental vapor pressures and calculated vapor pressures based on
263 Aspen using built-in correlations for solid – gas equilibrium is illustrated in Fig. 2. The
264 experimental values of vapor pressures for temperatures lower than the triple point for
265 fluoranthene [32], naphthalene [33] and phenol [34] were taken from literature studies. The
266 agreement between the experimental values and the calculated ones shown in Fig. 2 indicates the
267 possibility of extending the correlations used for gas and liquid phases to cover the solid phase. It
268 should be mentioned that the vapor pressure taken from the literature review are for mixtures of
269 fluoranthene, naphthalene and phenol in air and not in producer gas. This might lead to a certain
270 deviation between calculated and experimental vapor pressure values.

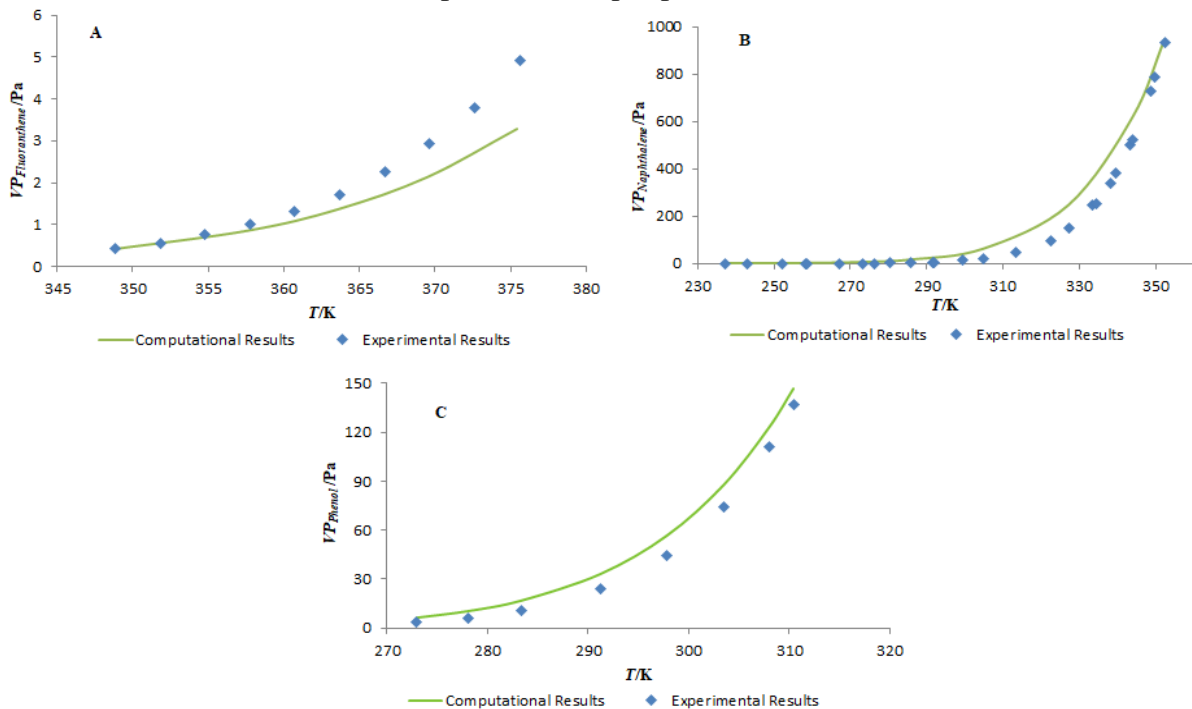


Fig. 2. Comparison between the experimental vapor pressures (VP) and the calculated ones based on Aspen correlations for A) fluoranthene [32], B) naphthalene [33] and C) phenol [34] at temperatures lower than the triple point.

271 **3.2. Tar dew point**

272 After validating that the correlations of Aspen could be extended to cover also the solid - gas
273 equilibrium, the dew point of tar representative components can be calculated. A comparison
274 between the calculated dew point of those components and the ones retrieved from the ECN tool
275 is completed. The different cases summarized previously in Table 3 are considered to check the
276 impact of the producer gas composition on tar condensation. The calculations are carried out for
277 a single tar component at a time. Fig. 3 groups all the results calculated for the different producer
278 gas compositions and compare them to the dew point obtained from the ECN online tool for the
279 same tar concentration. It can be observed from Fig. 3 that the dew point of tar components

280 varies according to the producer gas composition except for fluoranthene. Note that by
 281 decreasing the temperature, tar and water initially contained in the producer gas are both being
 282 condensed.

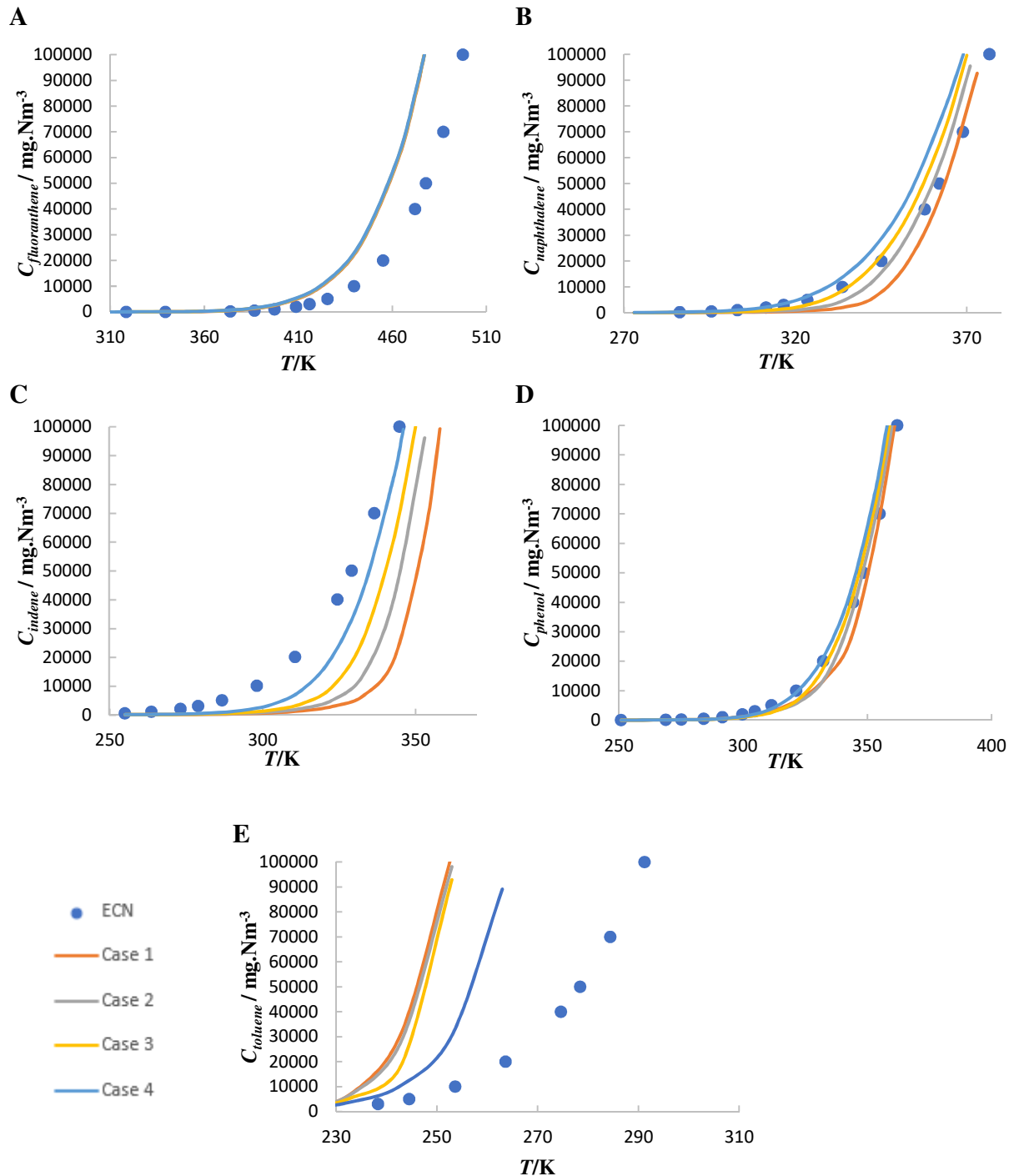


Fig. 3. Dew point of A) fluoranthene, B) naphthalene, C) indene, D) phenol and E) toluene in producer gas mixtures for different compositions.

283 The dew point of fluoranthene (Fig. 3 A) is expected to be the highest one since this latter is the
284 heaviest component. ECN stated that their online tool overestimates the dew point of tar by 7 to
285 14 K at temperature higher than 440 K. This explains the large deviation between the dew points
286 calculated and those obtained from their online tool at high temperatures. The major part of
287 fluoranthene is removed by condensation before reaching water dew point. The latter depends on
288 the initial moisture content (described in Table 3) varying from 303 to 333 K. It can be
289 concluded that the dew point of tar components is mainly affected by the moisture content and
290 the condensation of steam in the producer gas rather than the composition of the non-
291 condensable gases.

292 The dew points of naphthalene (Fig. 3 B), indene (Fig. 3 C) and phenol (Fig. 3 D) decrease with
293 the initial moisture content. While for toluene (Fig. 3 E), the higher the initial moisture content,
294 the lower the toluene dew point. Contrary to other tar representative components, toluene with
295 water forms an azeotropic mixture leading to a decrease in the boiling point. This explain the
296 difference in the behavior between toluene and the rest of tar components regarding the variation
297 of the initial moisture content present in the producer gas. The best agreement between the
298 calculated dew point and the ones available online is encountered for phenol and naphthalene.
299 Indene shows a high deviation for high moisture content. The deviation decreases for a low
300 moisture content in the producer gas (6 mol %_{wet}). The same analogy applies for the toluene. The
301 highest deviation is faced for Case 1 which corresponds to the highest moisture content (30.4
302 mol %_{wet}). The lowest deviation is achieved for Case 4 having the lowest initial moisture content.
303 Although the deviation decreases with the initial moisture content for toluene, the difference is
304 still high. This may be caused by ice formation at temperatures lower than 273 K.

305 As seen, tar dew point depends on the composition of the producer gas. However, this
306 composition is not defined for the online tool calculator. It is only mentioned that their tool is
307 based on an atmospheric bubbling fluidized bed operating at 1123 K using air as a gasification
308 agent. All these factors increase the deviation between the calculated tar dew points and those
309 obtained through the online dew point calculator.

310 **3.3. Psychrometric charts**

311 By completing the calculations for all the mixtures of tar representative components in the raw
312 gas, psychrometric charts for tar-raw gas mixtures were plotted. Calculations in this section are
313 based on Case 1 in Table 3 referring to a DFB gasifier. The latter is selected since it yields a
314 suitable producer gas composition for methanation. The five psychrometric charts of
315 fluoranthene, naphthalene, indene, phenol and toluene – raw gas mixtures are illustrated in Fig.
316 4, Fig. 5, Fig. 6, Fig. 7 and Fig. 8, respectively. The aim is to obtain a raw gas with a tar content
317 lower than 1 mg.Nm⁻³. It can be deduced that a temperature around 193 K is required to reach it.
318 Note that the enthalpy difference calculated between two points is more significant than the one
319 calculated at each point since it reflects the required energy for condensing a certain mass of tars.
320 To find the enthalpy of a point on the charts that is not at saturation, the isenthalpic lines are
321 projected until they reach the enthalpy line at saturation (bold black dashed line). The
322 intersection between the projection and the enthalpy at saturation line is then read on the right

323 axis. This value corresponds to the enthalpy in kJ.kg^{-1} . In Fig. 4, Fig. 5, Fig. 6, Fig. 7 and Fig. 8,
 324 the light grey lines represent the projection of the isenthalpic lines for better understanding.
 325 At a tar content of 100 g.Nm^{-3} , the condensation of water and the tar representative component
 326 take place simultaneously, except for the heaviest one (fluoranthene) and the lightest one
 327 (toluene). The condensation of fluoranthene, toluene and water starts at a temperature of 476 K,
 328 253 K and 355 K, respectively. In other words, fluoranthene condenses prior to water while
 329 toluene condenses after it. It can be deduced, from the figures below, that the condensation of
 330 water has a higher impact on the enthalpy change. This is justified by the increase in the slope of
 331 the enthalpy for temperatures lower than that of water dew point. According to Fig. 4, the
 332 enthalpy varies linearly function of temperatures greater than 355 K. This section presents the
 333 condensation of fluoranthene only. Below this temperature, water condensation starts, leading to
 334 a higher enthalpy variation thus a steeper enthalpy slope. Moreover, the water fraction is higher
 335 than the tar fraction in the producer gas, thus the impact of water condensation on the enthalpy is
 336 higher. Moving to indene, naphthalene and phenol, the slope of the enthalpy is notably higher
 337 than that of fluoranthene. According to Fig. 4 and Fig. 6, to reduce the tar content (w) from 0.06
 338 to 0.02 kg.kg^{-1} , the energy required for fluoranthene is equal to 98.7 kJ.kg^{-1} while that of indene
 339 is much higher (217.4 kJ.kg^{-1}). Finally, the condensation of toluene begins after the removal of a
 340 high fraction of water. As a result, the energy required for toluene condensation to reduce the
 341 content from 0.06 to 0.02 kg.kg^{-1} is the lowest one ($28.519 \text{ kJ.kg}^{-1}$), as seen in Fig. 8.

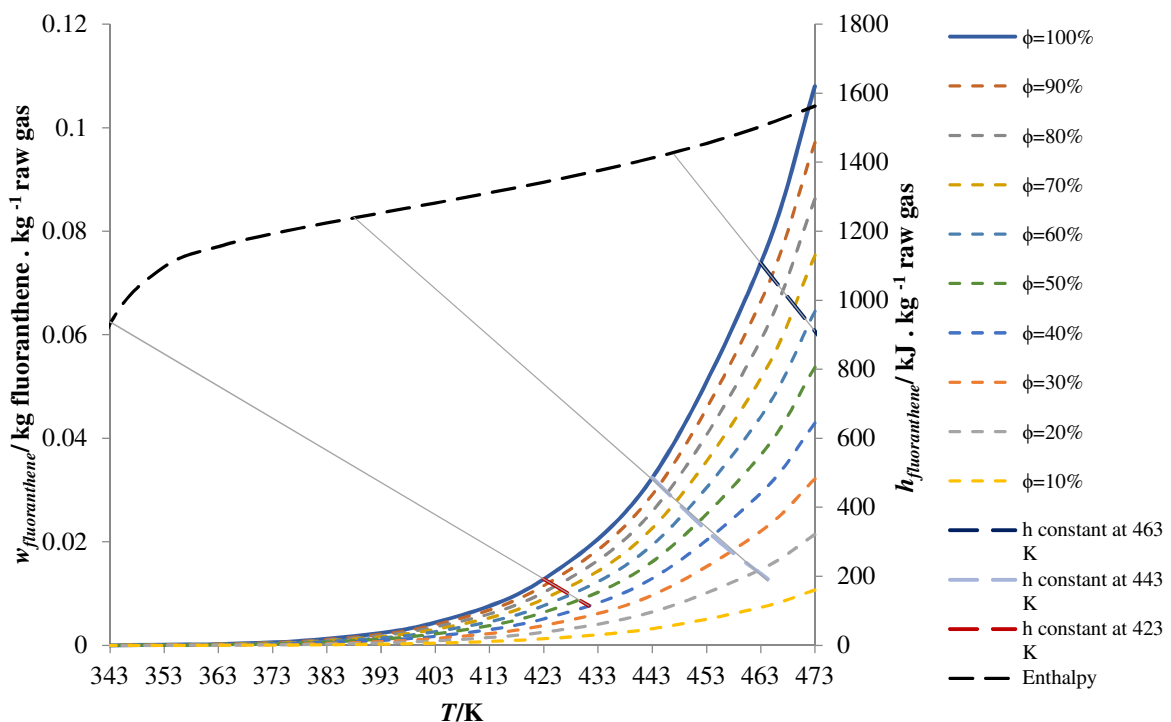


Fig. 4. Psychrometric charts of fluoranthene-raw gas mixture.

342

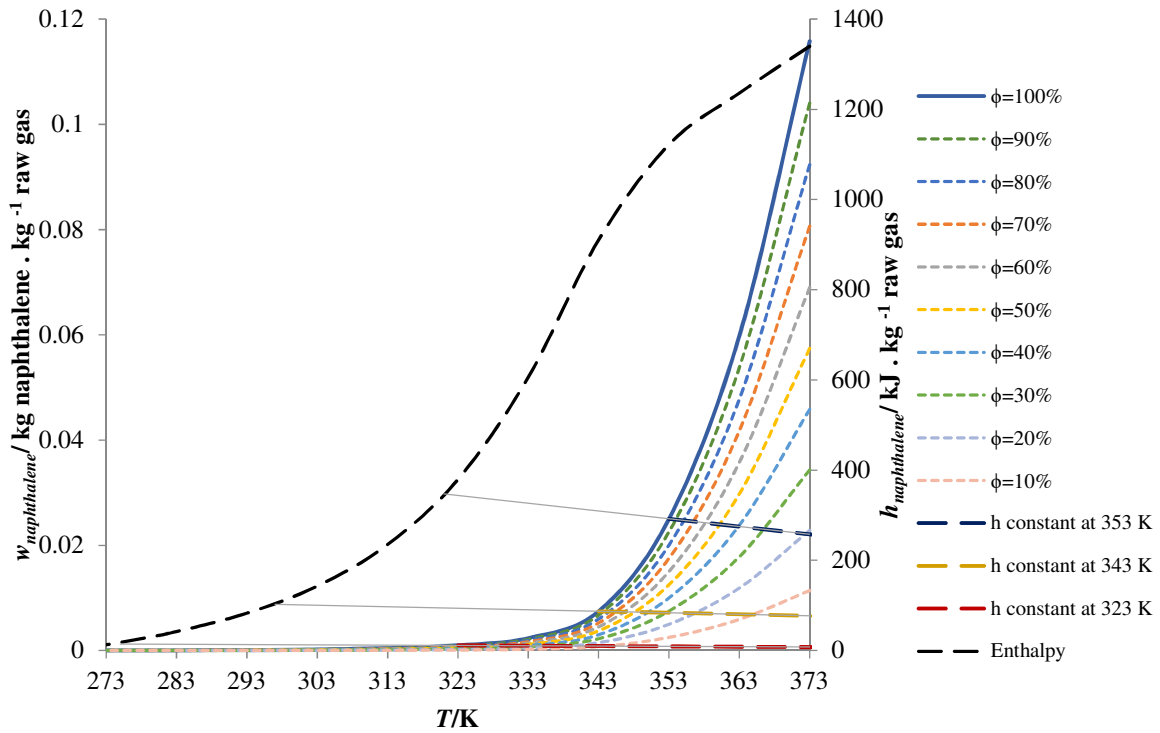


Fig. 5. Psychrometric charts of naphthalene-raw gas mixture.

343

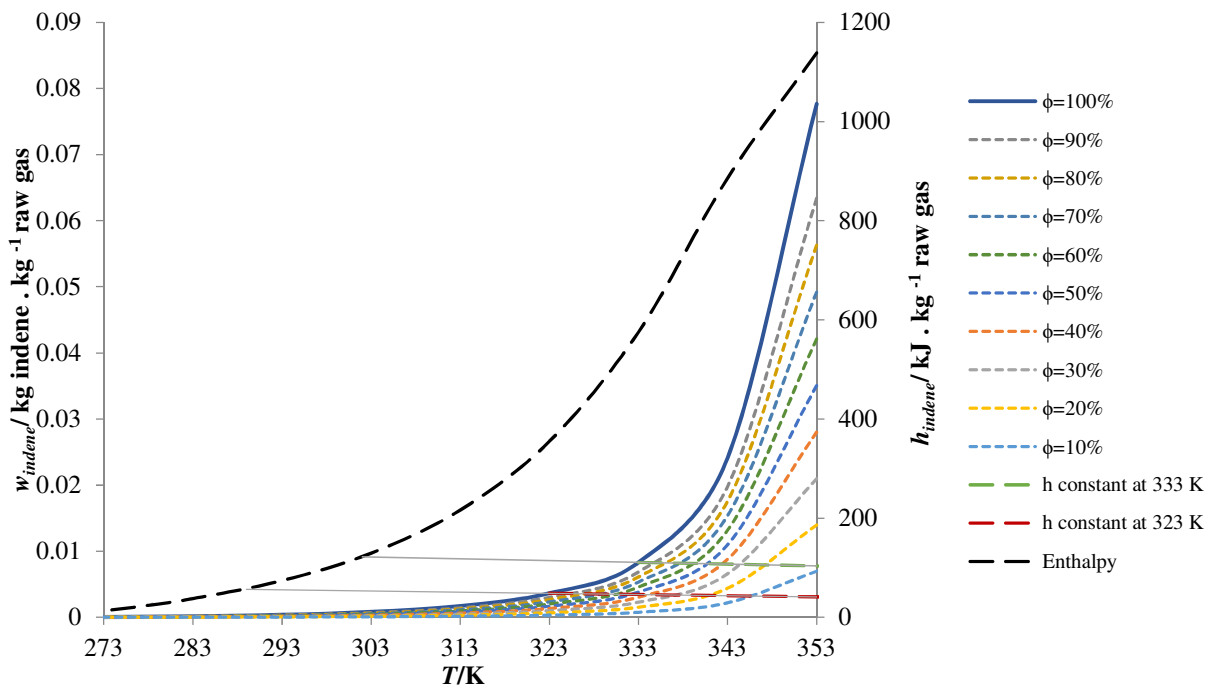


Fig. 6. Psychrometric charts of indene-raw gas mixture.

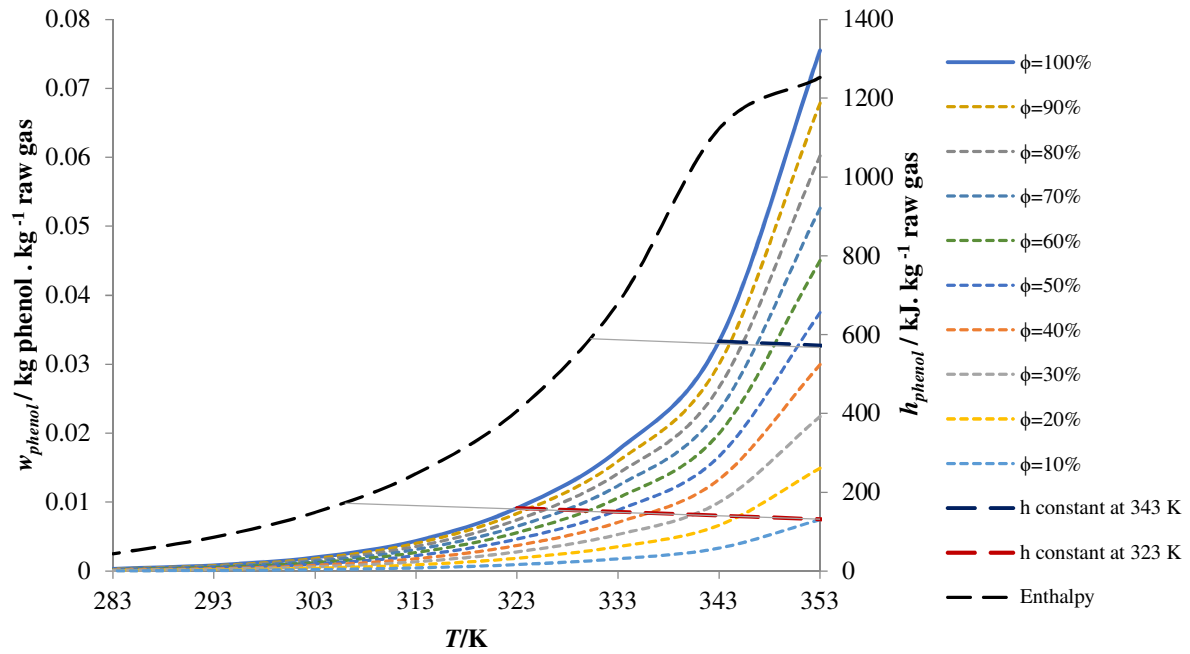


Fig. 7. Psychrometric charts of phenol-raw gas mixture.

344

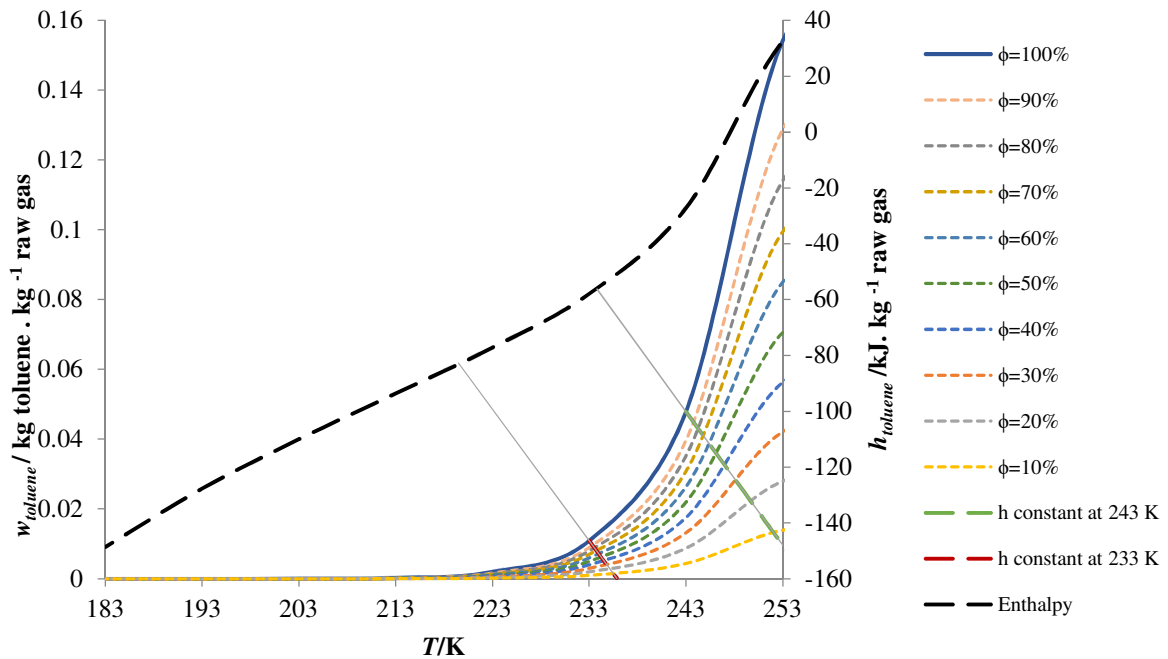


Fig. 8. Psychrometric charts of toluene-raw gas mixture.

345 We can observe in Fig. 4, Fig. 5, Fig. 6, Fig. 7 and Fig. 8 that, at low temperatures, the charts
 346 have very small values and therefore, the tar content is not readable. Table 4, Table 5, Table 6,
 347 Table 7 and Table 8 present the tar content and the enthalpy of fluoranthene, naphthalene,

348 indene, phenol and toluene in function of temperature. The more accurate values may be of a
 349 great benefit for those working with gasification and tar removal by physical methods.
 350 Moreover, they reflect the required temperature for reaching the limit for any application, not
 351 only for biomethane production. The values presented in the tables below correspond to the
 352 saturation line where $\phi=100\%$.

353 **Table 4**
 354 Computational mass content (w), concentration (C) and enthalpy (h) at temperature (T) and atmospheric pressure for the mixture
 355 of fluoranthene in raw gas.

T / K	$C_{\text{fluoranthene}} / \text{mg.Nm}^{-3}$	$w_{\text{fluoranthene}} / \times 10^{-5} \text{ kg.kg}^{-1}$ raw gas	$h_{\text{fluoranthene}} / \text{kJ. kg}^{-1}$ raw gas	T / K	$C_{\text{fluoranthene}} / \text{mg.Nm}^{-3}$	$w_{\text{fluoranthene}} / \times 10^{-5} \text{ kg.kg}^{-1}$ raw gas	$h_{\text{fluoranthene}} / \text{kJ. kg}^{-1}$ raw gas
393.15	1950.30	244.24	1277.07	359.15	136.62	17.27	1156.64
391.15	1719.08	215.32	1271.17	357.15	109.78	13.90	1144.97
389.15	1511.45	189.34	1265.25	355.15	86.88	11.03	1131.51
387.15	1325.35	166.06	1259.28	351.15	51.31	6.56	1095.98
385.15	1158.86	145.23	1253.25	349.15	38.00	4.88	1071.31
383.15	1010.19	126.63	1247.16	345.15	19.20	2.51	998.15
381.15	877.86	110.08	1240.98	343.15	13.26	1.76	946.38
379.15	760.38	95.37	1234.70	339.15	6.42	0.88	819.66
377.15	656.28	82.35	1228.29	337.15	4.61	0.65	752.77
375.15	564.24	70.82	1221.73	335.15	3.39	0.48	687.98
373.15	483.03	60.66	1214.98	333.15	2.54	0.37	626.96
369.15	348.78	43.85	1200.73	331.15	1.94	0.29	570.43
367.15	293.82	36.96	1193.10	329.15	1.50	0.23	518.54
365.15	245.83	30.95	1185.03	327.15	1.17	0.18	471.15
361.15	167.87	21.18	1167.00	325.15	0.93	0.14	427.97

356 **Table 5**
 357 Computational mass content (w), concentration (C) and enthalpy (h) at temperature (T) and atmospheric pressure for the mixture
 358 of naphthalene in raw gas.

T / K	$C_{\text{naphthalene}} / \text{mg.Nm}^{-3}$	$w_{\text{naphthalene}} / \times 10^{-5} \text{ kg.kg}^{-1}$ raw gas	$h_{\text{naphthalene}} / \text{kJ. kg}^{-1}$ raw gas	T / K	$C_{\text{naphthalene}} / \text{mg.Nm}^{-3}$	$w_{\text{naphthalene}} / \times 10^{-5} \text{ kg.kg}^{-1}$ raw gas	$h_{\text{naphthalene}} / \text{kJ. kg}^{-1}$ raw gas
330.15	1196.61	179.20	527.70	285.15	33.80	5.86	49.18
327.15	902.32	138.01	458.47	282.15	26.65	4.63	38.82
324.15	691.93	107.84	397.86	279.15	20.93	3.64	29.41
321.15	537.34	85.14	345.00	276.15	16.37	2.86	20.83
318.15	421.21	67.71	298.96	273.15	12.75	2.23	12.94
315.15	332.45	54.12	258.83	270.15	9.89	1.73	5.65
312.15	263.68	43.40	223.82	267.15	7.62	1.34	-1.15
309.15	209.83	34.87	193.22	264.15	5.85	1.03	-7.53
306.15	167.32	28.04	166.44	261.15	4.46	0.78	-13.56
303.15	133.55	22.54	142.93	258.15	3.38	0.60	-19.30
300.15	106.61	18.10	122.26	255.15	2.55	0.45	-24.80
297.15	85.04	14.52	104.01	252.15	1.91	0.34	-30.10
294.15	67.75	11.62	87.85	249.15	1.42	0.25	-35.24
291.15	53.87	9.28	73.50	246.15	1.04	0.18	-40.24
288.15	42.74	7.38	60.68	245.15	0.95	0.17	-41.88

359

360
361
362

Table 6

Computational mass content (w), concentration (C) and enthalpy (h) at temperature (T) and atmospheric pressure for the mixture of indene in raw gas.

T / K	$C_{\text{indene}} / \text{mg.Nm}^{-3}$	$w_{\text{indene}} / \times 10^{-5} \text{ kg.kg}^{-1}$	$h_{\text{indene}} / \text{kJ. kg}^{-1}$	T / K	$C_{\text{indene}} / \text{mg.Nm}^{-3}$	$w_{\text{indene}} / \times 10^{-5} \text{ kg.kg}^{-1}$	$h_{\text{indene}} / \text{kJ. kg}^{-1}$
		raw gas	raw gas			raw gas	raw gas
310.15	839.82	139.19	185.89	272.15	37.86	6.62	10.81
308.15	721.50	120.28	167.86	270.15	31.42	5.50	6.86
306.15	619.87	103.89	151.42	268.15	26.02	4.56	3.13
302.15	457.03	77.31	122.71	266.15	21.48	3.77	-0.40
300.15	392.01	66.58	110.18	264.15	17.69	3.11	-3.77
298.15	335.90	57.25	98.71	262.15	14.53	2.55	-6.98
294.15	245.66	42.13	78.57	260.15	11.90	2.09	-10.05
292.15	209.59	36.05	69.73	256.15	7.91	1.39	-15.85
290.15	178.50	30.77	61.59	254.15	6.42	1.13	-18.60
288.15	151.73	26.22	54.10	252.15	5.19	0.92	-21.27
286.15	128.70	22.28	47.19	250.15	4.18	0.74	-23.87
284.15	108.91	18.89	40.80	246.15	2.69	0.48	-28.88
280.15	77.43	13.47	29.38	244.15	2.15	0.38	-31.31
278.15	65.03	11.33	24.26	240.15	1.35	0.24	-36.04
274.15	45.48	7.94	15.01	237.15	0.94	0.17	-39.50

363

364

365
366
367

Table 7

Computational mass content (w), concentration (C) and enthalpy (h) at temperature (T) and atmospheric pressure for the mixture of phenol in raw gas.

T / K	$C_{\text{phenol}} / \text{mg.Nm}^{-3}$	$w_{\text{phenol}} / \times 10^{-5} \text{ kg.kg}^{-1}$	$h_{\text{phenol}} / \text{kJ. kg}^{-1}$	T / K	$C_{\text{phenol}} / \text{mg.Nm}^{-3}$	$w_{\text{phenol}} / \times 10^{-5} \text{ kg.kg}^{-1}$	$h_{\text{phenol}} / \text{kJ. kg}^{-1}$
		raw gas	raw gas			raw gas	raw gas
303.15	1159.37	195.91	118.15	271.15	52.52	9.26	8.52
301.15	975.65	165.62	106.17	269.15	42.05	7.42	3.74
299.15	819.18	139.64	95.08	267.15	33.54	5.93	-0.83
297.15	686.16	117.42	84.81	265.15	26.63	4.72	-5.21
295.15	573.32	98.45	75.29	263.15	21.06	3.73	-9.43
293.15	477.79	82.31	66.45	261.15	16.58	2.94	-13.49
291.15	397.11	68.61	58.22	259.15	12.99	2.31	-17.41
289.15	329.12	57.01	50.55	257.15	10.13	1.80	-21.23
287.15	271.97	47.23	43.38	255.15	7.86	1.40	-24.93
285.15	224.07	39.00	36.67	253.15	6.07	1.08	-28.55
283.15	184.02	32.10	30.37	251.15	4.66	0.83	-32.09
281.15	150.64	26.33	24.44	249.15	3.56	0.64	-35.56
279.15	122.90	21.52	18.85	247.15	2.70	0.49	-38.96
277.15	99.91	17.53	13.55	245.15	2.04	0.37	-42.32
275.15	80.94	14.22	118.15	243.15	1.53	0.28	-45.62
273.15	65.32	11.50	106.17	240.15	0.99	0.18	-50.51

368

369

370
371
372

Table 8

Computational mass content (w), concentration (C) and enthalpy (h) at temperature (T) and atmospheric pressure for the mixture of toluene in raw gas.

T / K	$C_{toluene} /$ $mg.Nm^{-3}$	$w_{toluene} /$ $x10^{-5} kg.kg^{-1}$	$h_{toluene} /$ $kJ. kg^{-1}$	T / K	$C_{toluene} /$ $mg.Nm^{-3}$	$w_{toluene} /$ $x10^{-5} kg.kg^{-1}$	$h_{toluene} /$ $kJ. kg^{-1}$
		raw gas	raw gas			raw gas	raw gas
223.15	1076.46	197.84	-75.24	209.15	44.90	8.41	-96.65
222.15	887.42	163.26	-76.86	208.15	34.25	6.43	-98.12
221.15	728.20	134.10	-78.47	207.15	25.96	4.88	-99.59
220.15	594.70	109.64	-80.05	206.15	19.54	3.68	-101.05
219.15	483.29	89.20	-81.61	205.15	14.61	2.76	-102.52
218.15	390.77	72.20	-83.16	204.15	10.85	2.05	-103.97
217.15	314.32	58.15	-84.69	203.15	8.00	1.52	-105.43
216.15	251.47	46.58	-86.21	202.15	5.85	1.11	-106.89
215.15	200.09	37.11	-87.73	201.15	4.25	0.81	-108.34
214.15	158.31	29.41	-89.23	200.15	3.07	0.59	-109.80
213.15	124.54	23.17	-90.73	199.15	2.20	0.42	-111.25
212.15	97.40	18.15	-92.21	198.15	1.56	0.30	-112.70
211.15	75.71	14.13	-93.70	197.15	1.10	0.21	-114.15
210.15	58.49	10.93	-95.18	196.15	0.77	0.15	-115.59

373 The enthalpy variation is caused by three different processes. The latent heat of the tar
374 component condensation, the latent heat of the water condensation and the sensible heat of the
375 gas. For fluoranthene (Table 4), the variation of the enthalpy at high temperature for $433 K \leq$
376 $T \leq 473 K$, is driven by the latent heat of fluoranthene condensation, where 83% of the initial
377 fluoranthene content is condensed. For temperatures ranging between 355 K and 433 K, the
378 sensible heat of the gas occupies the major fraction of the enthalpy variation. Below 355 K, the
379 enthalpy variation is driven by the latent heat of water condensation. For naphthalene (Table 5),
380 indene (Table 6) and phenol (Table 7), the latent heat of the tar component surpasses the rest for
381 temperatures higher than 355 K. Between 355 K and 283 K, the latent heat of water condensation
382 forms the major part of the enthalpy variation. Below 283 K, the sensible heat surpasses both
383 latent heats. For toluene (Table 8), since its condensation starts below 273 K, the latent heat of
384 toluene condensation drives the enthalpy variation for temperatures higher than 243 K. Below
385 this temperature, the weight of the sensible heat on the enthalpy variation becomes greater than
386 the latent heat.

387 It can be seen that fluoranthene is the first tar representative component that reaches a
388 concentration of $1 mg.Nm^{-3}$ at a temperature of 325.15 K. On the other hand, toluene is the last
389 tar representative component reaching $1 mg.Nm^{-3}$ at 196.15 K. Finally, the temperatures for
390 indene, naphthalene and phenol, required to reach a concentration of $1 mg.Nm^{-3}$, are 237.15 K,
391 245.15 K and 240.15 K, respectively. As a conclusion, toluene is the last component reduced to a
392 concentration of $1 mg.Nm^{-3}$ since it requires the lowest temperature.

393 **4. Conclusion**

394 In this paper, four different producer gas compositions were studied to check their impact on tar
395 removal. The study involves the calculation of the dew point of several components besides
396 water, that are fluoranthene, naphthalene, indene, phenol and toluene. Each component was
397 separately studied with the producer gas. The dew point was calculated for tar concentrations
398 ranging between 0.001 and 100 g.Nm⁻³. Psychrometric charts were plotted for the gas
399 composition of dual fluidized bed gasifier to represent gas stream thermodynamic properties
400 variations during tar capture by applying low temperatures. As a result, the dew points of
401 fluoranthene, naphthalene, indene, phenol and toluene vary respectively from 325 to 473 K, 245
402 to 374 K, 237 to 359 K, 240 to 361 K and 196 to 262 K. In addition, the high level of required
403 energy for tar removal at temperature lower than the water dew point is a result of water
404 existence in the producer gas. As for future work, we aim at using the obtained results to study
405 the condensation of tar on a vertical plate surface, which could be beneficial in evaluating the tar
406 and water removal efficiency.

407 **Nomenclature**

C	Concentration, mg.Nm ⁻³
C_p	Vapor heat capacity, kJ.kg ⁻¹ .K ⁻¹
ER	Equivalence ratio
h	Enthalpy, kJ.kg ⁻¹
h_{fg}	Latent heat of vaporization, kJ.kg ⁻¹
m	Mass, kg
M	Molecular masses, g.mol ⁻¹
P_{sat}	Saturation tar partial pressures, Pa
P_{tar}	Tar partial pressure, Pa
P_{total}	Total mixture pressure, Pa
T	Temperature, K
VF	Vapor fraction
VP	Vapor pressure, Pa
w_{tar}	Tar content, kg.kg ⁻¹
y	Vapor phase mole fraction

Greek symbols

ϕ	Tar relative concentration
ρ	Density, kg.m ⁻³

Subscripts

DB	Dry bulb
DP	Dew point
j	Raw gas component
tar	Tar representative component
wat	Water

Abbreviations

CHP	Combined Heat and Power
DFB	Dual Fluidized Bed
ECN	Energy research Center of the Netherlands
RDF	Refused-Derived Fuel

409 **References**

- 410 [1] Patra TK, Mukherjee S, Sheth PN. Process simulation of hydrogen rich gas production from
411 producer gas using HTS catalysis. *Energy* 2019;173:1130–40.
412 <https://doi.org/10.1016/j.energy.2019.02.136>.
- 413 [2] Anis S, Zainal ZA. Tar reduction in biomass producer gas via mechanical, catalytic and
414 thermal methods: A review. *Renewable and Sustainable Energy Reviews* 2011;15:2355–77.
415 <https://doi.org/10.1016/j.rser.2011.02.018>.
- 416 [3] Valderrama Rios ML, González AM, Lora EES, Almazán del Olmo OA. Reduction of tar
417 generated during biomass gasification: A review. *Biomass and Bioenergy* 2018;108:345–
418 70. <https://doi.org/10.1016/j.biombioe.2017.12.002>.
- 419 [4] de Lasa H, Salaiques E, Mazumder J, Lucky R. Catalytic steam gasification of biomass:
420 catalysts, thermodynamics and kinetics. *Chemical Reviews* 2011;111:5404–33.
421 <https://doi.org/10.1021/cr200024w>.
- 422 [5] Zhang Y, Kajitani S, Ashizawa M, Oki Y. Tar destruction and coke formation during rapid
423 pyrolysis and gasification of biomass in a drop-tube furnace. *Fuel* 2010;89:302–9.
424 <https://doi.org/10.1016/j.fuel.2009.08.045>.
- 425 [6] Guan G, Kaewpanha M, Hao X, Abudula A. Catalytic steam reforming of biomass tar:
426 Prospects and challenges. *Renewable and Sustainable Energy Reviews* 2016;58:450–61.
427 <https://doi.org/10.1016/j.rser.2015.12.316>.
- 428 [7] Woolcock PJ, Brown RC. A review of cleaning technologies for biomass-derived syngas.
429 *Biomass and Bioenergy* 2013;52:54–84. <https://doi.org/10.1016/j.biombioe.2013.02.036>.
- 430 [8] Maniatis K, Beenackers AACM. Tar Protocols. IEA Bioenergy Gasification Task. *Biomass*
431 *and Bioenergy* 2000;18:1–4. [https://doi.org/10.1016/S0961-9534\(99\)00072-0](https://doi.org/10.1016/S0961-9534(99)00072-0).
- 432 [9] Weston PH. Tar Destruction in a Coandă Tar Cracker. The University of Sheffield, 2014.
- 433 [10] Bermudez JM, Fidalgo B. Production of bio-syngas and bio-hydrogen via gasification. In:
434 Luque R, Lin CSK, Wilson K, Clark J, editors. *Handbook of Biofuels Production*. Second
435 Edition, Woodhead Publishing; 2016, p. 431–94. <https://doi.org/10.1016/B978-0-08-100455-5.00015-1>.
- 436 [11] Phuphuakrat T, Namioka T, Yoshikawa K. Absorptive removal of biomass tar using water
437 and oily materials. *Bioresource Technology* 2011;102:543–9.
438 <https://doi.org/10.1016/j.biortech.2010.07.073>.
- 439 [12] Zwart RWR, Van der Drift A, Bos A, Visser HJM, Cieplik MK, Könemann HWJ. Oil-
440 based gas washing-Flexible tar removal for high-efficient production of clean heat and
441 power as well as sustainable fuels and chemicals. *Environmental Progress Sustainable &*
442 *Energy* 2009;28:324–35. <https://doi.org/10.1002/ep.10383>.
- 443 [13] Brandt P, Henriksen U. Decomposition of tar in gas from updraft gasifier by thermal
444 cracking. 1st World Conference and Exhibition on Biomass for Energy and Industry, Spain:
445 James & James; 2000, p. 4.
- 446 [14] Lu P, Huang Q, Bourtsalac AC, Chi Y, Yan J. Effect of operating conditions on the coke
447 formation and nickel catalyst performance during cracking of tar. *Waste and Biomass*
448 *Valorization* 2019;10:155–65. <https://doi.org/10.1007/s12649-017-0044-5>.
- 449 [15] Pallozzi V, Di Carlo A, Bocci E, Carlini M. Combined gas conditioning and cleaning for
450 reduction of tars in biomass gasification. *Biomass and Bioenergy* 2018;109:85–90.
451 <https://doi.org/10.1016/j.biombioe.2017.12.023>.
- 452

- 453 [16] Boerrigter H. “OLGA” tar removal technology: Proof of-concept for application in
454 integrated biomass gasification combined heat and power (CHP) systems. *ECN Biomass*
455 2005:58.
- 456 [17] Thunman H, Seemann M, Vilches TB, Maric J, Pallares D, Ström H, et al. Advanced
457 biofuel production via gasification – lessons learned from 200 man-years of research
458 activity with Chalmers’ research gasifier and the GoBiGas demonstration plant. *Energy*
459 *Science & Engineering* 2018;6:6–34. <https://doi.org/10.1002/ese3.188>.
- 460 [18] Phuphuakrat T, Namioka T, Yoshikawa K. Tar removal from biomass pyrolysis gas in two-
461 step function of decomposition and adsorption. *Applied Energy* 2010;87:2203–11.
462 <https://doi.org/10.1016/j.apenergy.2009.12.002>.
- 463 [19] Pallozzi V, Di Carlo A, Bocci E, Carlini M. Combined gas conditioning and cleaning for
464 reduction of tars in biomass gasification. *Biomass and Bioenergy* 2018;109:85–90.
465 <https://doi.org/10.1016/j.biombioe.2017.12.023>.
- 466 [20] Thersites: Complete model. <http://www.thersites.nl/completemodel.aspx> (accessed July 18,
467 2019).
- 468 [21] Rabou LPLM, Zwart RWR, Vreugdenhil BJ, Bos L. Tar in biomass producer gas, the
469 energy research centre of the netherlands (ECN) experience: an enduring challenge. *Energy*
470 *& Fuels* 2009;23:6189–98. <https://doi.org/10.1021/ef9007032>.
- 471 [22] AspenTech. *Aspen Physical Property Methods* 2013.
- 472 [23] Alamia A, Larsson A, Breitholtz C, Thunman H. Performance of large-scale biomass
473 gasifiers in a biorefinery, a state-of-the-art reference. *International Journal of Energy*
474 *Research* 2017;41:2001–19. <https://doi.org/10.1002/er.3758>.
- 475 [24] Abu El-Rub Z, Bramer EA, Brem G. Experimental comparison of biomass chars with other
476 catalysts for tar reduction. *Fuel* 2008;87:2243–52.
477 <https://doi.org/10.1016/j.fuel.2008.01.004>.
- 478 [25] Schmid M, Beirow M, Schweitzer D, Waizmann G, Spörl R, Scheffknecht G. Product gas
479 composition for steam-oxygen fluidized bed gasification of dried sewage sludge, straw
480 pellets and wood pellets and the influence of limestone as bed material. *Biomass and*
481 *Bioenergy* 2018;117:71–7. <https://doi.org/10.1016/j.biombioe.2018.07.011>.
- 482 [26] Myrén C, Hörnell C, Björnbom E, Sjöström K. Catalytic tar decomposition of biomass
483 pyrolysis gas with a combination of dolomite and silica. *Biomass and Bioenergy*
484 2002;23:217–27. [https://doi.org/10.1016/S0961-9534\(02\)00049-1](https://doi.org/10.1016/S0961-9534(02)00049-1).
- 485 [27] Han J, Kim H. The reduction and control technology of tar during biomass
486 gasification/pyrolysis: An overview. *Renewable and Sustainable Energy Reviews*
487 2008;12:397–416. <https://doi.org/10.1016/j.rser.2006.07.015>.
- 488 [28] van der Meijden C, Könemann J-W, Sierhuis W, van der Drift B, Rietveld B. Wood to Bio-
489 Methane demonstration project in the Netherlands. *Energy Research Centre of the*
490 *Netherlands (ECN)* 2013:13.
- 491 [29] Gil J, Corella J, Aznar MP, Caballero MA. Biomass gasification in atmospheric and
492 bubbling fluidized bed: Effect of the type of gasifying agent on the product distribution.
493 *Biomass and Bioenergy* 1999;17:389-403. [https://doi.org/10.1016/S0961-9534\(99\)00055-0](https://doi.org/10.1016/S0961-9534(99)00055-0).
- 494 [30] van Paasen SVB, Cieplik MK, Phokawat NP. *Gasification of Non-woody Biomass*. Energy
495 research Centre of the Netherlands; 2006.
- 496 [31] Hassan S, Zainal ZA, Miskam MA. A preliminary investigation of compressed producer
497 gas from downdraft biomass gasifier. *Journal of Applied Sciences* 2010;10:406–12.
498 <http://dx.doi.org/10.3923/jas.2010.406.412>.

- 499 [32] Monte MJS, Notario R, Pinto SP, Lobo Ferreira AIMC, Ribeiro da Silva MDMC.
500 Thermodynamic properties of fluoranthene: An experimental and computational study. *The*
501 *Journal of Chemical Thermodynamics* 2012;49:159–64.
502 <https://doi.org/10.1016/j.jct.2012.01.025>.
- 503 [33] de Kruif CG, Kuipers T, van Miltenburg JC, Schaake RCF, Stevens G. The vapour pressure
504 of solid and liquid naphthalene. *The Journal of Chemical Thermodynamics* 1981;13:1081–
505 6. [https://doi.org/10.1016/0021-9614\(81\)90006-9](https://doi.org/10.1016/0021-9614(81)90006-9).
- 506 [34] Biddiscombe DP, Martin JF. Vapour pressures of phenol and the cresols. *Transactions of*
507 *the Faraday Society* 1958;54:1316. <https://doi.org/10.1039/tf9585401316>.
- 508
- 509

